

## Article

# Design and Analysis of an Optical–Acoustic Cooperative Communication System for an Underwater Remote-Operated Vehicle <sup>†</sup>

Jun He <sup>1</sup>, Jie Li <sup>1</sup>, Xiaowu Zhu <sup>2,\*</sup>, Shangkun Xiong <sup>3</sup> and Fangjiong Chen <sup>1</sup> 

<sup>1</sup> School of Electronics and Information, South China University of Technology, Guangzhou 510641, China; 202021012588@mail.scut.edu.cn (J.H.); eeji@scut.edu.cn (J.L.); eefjchen@scut.edu.cn (F.C.)

<sup>2</sup> Surveying and Mapping Institute, Lands and Resource Department of Guangdong Province, Guangzhou 510599, China

<sup>3</sup> China Telecom Corp Ltd., Guangzhou 510641, China; xiongs@chinatelecom.cn

\* Correspondence: 13602728464@139.com; Tel.: +86-1360-272-8464

<sup>†</sup> This paper is an extended version of the paper published in He, J.; Wu, J.; Peng, Z.; Chen, F.; Yu, H.; Ji, F. Underwater Error-Free Data Transmission Based on Optical-Acoustic Cooperative Communication. In Proceedings of the 2021 IEEE/CIC International Conference on Communications in China (ICCC Workshops), Xiamen, China, 28–30 July 2021; pp. 211–216.

**Abstract:** Underwater wireless communication technology plays a key role in the field of marine equipment technology. In this paper, we experimentally demonstrate an underwater optical–acoustic cooperative communication platform for an underwater wireless data transmission system. The system utilizes an underwater Remote-Operated Vehicle (ROV) as a carrier, equipped with LEDbased optical communication and acoustic communication modems. In particular, the system applies optical communication to transmit large-scale data and applies acoustic communication to provide acoustic-assisted signaling exchange before optical transmission and Automatic Repeat Request (ARQ) during optical transmission. By experimentally measuring the transmission distance under different water quality conditions, we found that the system can achieve a data rate of up to 5 Mb/s over a laboratory underwater channel of 7.6 m. By comparing the attenuation coefficients for the outdoor underwater environment with that in clear seawater, we estimate that the achievable link distance in clear seawater can reach 11 m with a data rate of 3.125 MB/s. The proposed system takes both implementation complexity and cost into consideration and also provides significant guidance for future real-time high-speed underwater optical–acoustic communications.

**Keywords:** ROV; optical communication; acoustic communication; cooperative



**Citation:** He, J.; Li, J.; Zhu, X.; Xiong, S.; Chen, F. Design and Analysis of an Optical–Acoustic Cooperative Communication System for an Underwater Remote-Operated Vehicle. *Appl. Sci.* **2022**, *12*, 5533. <https://doi.org/10.3390/app12115533>

Academic Editor: Alexander Sutin

Received: 27 March 2022

Accepted: 22 May 2022

Published: 30 May 2022

**Publisher's Note:** MDPI stays neutral with regard to jurisdictional claims in published maps and institutional affiliations.



**Copyright:** © 2022 by the authors. Licensee MDPI, Basel, Switzerland. This article is an open access article distributed under the terms and conditions of the Creative Commons Attribution (CC BY) license (<https://creativecommons.org/licenses/by/4.0/>).

## 1. Introduction

With the increase in underwater activities, the development of marine resources has become particularly important. Underwater equipment such as Remote-Operated Vehicles (ROVs) and underwater robots are the main tools to explore marine resources and are widely used in the field of seismic acquisition. On the one hand, ROVs can automate nodal seafloor acquisition operations, and on the other hand, they can also retain the technical advantages of the ocean bottom node systems [1,2]. ROVs can be integrated into the Wi-buoy architecture so that low latency operation can be conducted in cells having a low arrival rate of packets [3]. As a key technology of underwater equipment, underwater wireless communication plays an important role. To transmit significant amounts of data without error, the demand for high-speed and reliable underwater data transmission keeps increasing [4,5]. In recent decades, many efforts have been made to find reliable and cost-effective communication methods [6,7]. Underwater acoustic communication (UAC) technology is the most mature and widely applied underwater communication technology, which has the advantages of long communication distance and high reliability. At the

same time, due to the slow propagation speed and narrow bandwidth of acoustic signals, acoustic communication technologies have the problems of low transmission rate and high transmission delay in long-distance communication [8,9]. Underwater visible light communication (UWVLC), which has the advantages of small system size and low energy consumption, can achieve a much higher transmission rate than UAC. However, due to the absorption, attenuation, and line-of-sight propagation characteristics of light, UWVLC systems usually require optical alignment to establish a reliable communication link [10,11].

In recent years, more and more attention has been paid to the communication methods of underwater equipment. A new modular underwater robot has been proposed in paper [12], which integrated a visible light communication (VLC) module into an underwater unmanned vehicle based on the UAC remote control. At the same time, the VLC modem transmits data at a rate of 320 kb/s. By loading an optical communication terminal on the submersible of their research institute, Norm Farr et al. realized real-time video transmission over a distance of 100 m at a bit rate of 1Mbps [13]. Pontbriand et al. have conducted many experiments to transmit 100 MB high-capacity data files between submarine nodes and autonomous underwater vehicles (AUV) at a bit rate of no more than 10 Mbps through a VLC modem. In their experiment, they transferred more than 5 GB files in 4.5 h and maintained the optical communication link in a cylindrical reliable communication range with a radius of 25–75 m and a depth of 125 m [14,15]. Their experimental results demonstrate the feasibility and superior performance of VLC in underwater mobile wireless communication applications.

In addition, long-term research also has been carried out on hybrid communication methods in underwater equipment. Seongwon Han et al. proposed optical communication for high-speed data communication over short distances, while UAC was used for long-distance control signal transmission and optical communication auxiliary alignment [16]. The simulation results showed that their hybrid communication scheme had higher throughput and energy efficiency. In 2019, they pointed out that when the optical communication link was stable, the video signal was directly transmitted; while, when the optical communication link was interrupted, the video signal was extracted into compressed static image frames by algorithms such as Sobel edge detection and Gaussian blurring and transmitted through underwater acoustic communication [17]. An underwater hybrid acoustic–optic communication scheme was proposed in [18]. Using a controller and a real-time acoustic positioning system, the AUV was guided to move to the underwater node where the acoustic and optical communication modems were installed, and the optical communication link was automatically established. The performance of the scheme was verified by simulation in terms of positioning time, communication link establishment time, and communication link recovery time. However, their work is still in the stage of simulation and analysis, and the actual acoustic–optic cooperative communication system has not been verified.

In this paper, an underwater optical–acoustic cooperative communication scheme that combines UWVLC with UAC is proposed from the perspective of enhancing the stability and reliability of underwater communication. This solution utilizes the advantages of long-distance, high-stability, and no strict line-of-sight transmission of UAC and provides auxiliary alignment and Automatic Repeat reQuest (ARQ) for optical communication. Moreover, we introduce channel coding into the optical–acoustic cooperative communication platform to improve the Bit Error Rate (BER) performance. Inspired by the traditional ARQ protocol, an error-free data transmission protocol for underwater optical–acoustic cooperative communication is proposed. The large-scale data are transmitted through optical communication, while the packet loss feedback function is realized by UAC. Hence, the system can achieve strong error control performance without establishing a bidirectional optical communication link. Based on our previous work [19], this paper describes the design and implementation of the underwater optical–acoustic cooperative communication platform in detail, the improvement the transmitting circuit, the experiment conducted in comparison with the previous circuit, and the addition of a BER monitor to monitor

the BER performance during transmission. In addition, we measured the communication distance under different water conditions and the BER at different transmitter offset angles. Based on the measurement results, we estimate that the achievable connection distance in clear water is about 11 m.

The rest of this paper is organized as follows. Section 2 describes the overall design of the system platform and clearly explains each structural unit. Section 3 describes the simulation of the proposed transmission protocol. The series of experiments carried out to examine the energy efficiency, BER performance, and transmission throughput of the system are described in Section 4. Finally, Section 5 provides concise conclusions on effective methods for designing underwater optical–acoustic cooperative communication platforms and improvements.

## 2. System Overview

The underwater optical–acoustic cooperative communication platform is designed and illustrated in Figure 1, which consists of several underwater dynamic communication nodes (ROV) and an underwater static communication node. The underwater static node, which can be tied to a boat or buoy, mainly includes three parts: a VLC module, a UAC module, and a data acquisition module. Different from the static node, the dynamic node also contains the motion control part of the ROV.

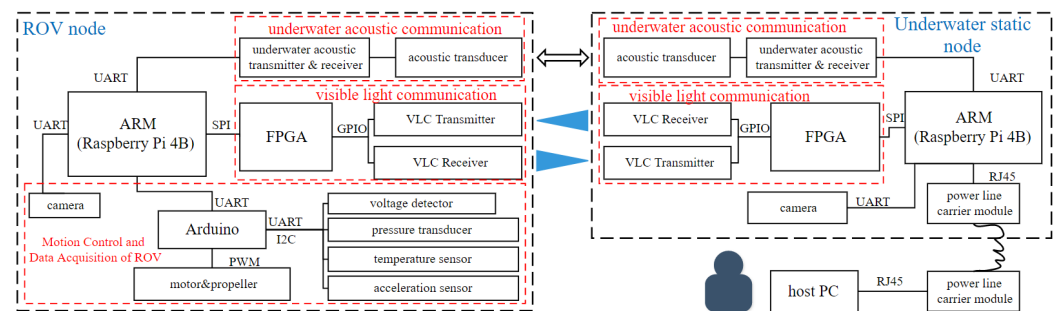


**Figure 1.** The basic composition diagram of optical–acoustic cooperative communication system.

### 2.1. VLC Transmitter

The transmitter mainly includes a modulation module, a light-emitting diode (LED) driving module, and a light source. After the field-programmable gate array (FPGA) processes the data, the visible light signal transmission circuit converts the electrical signal into a visible light signal, and transmits it to the underwater channel. Due to the serious attenuation of the underwater optical communication channel, a proper communication scheme must be designed to ensure that the UWVLC achieves a high transmission rate and long transmission distance.

We chose non-return-to-zero on–off keying (NRZ-OOK) as the signal modulation method of the system, where binary OOK directly modulates the binary digital baseband signal to the LED for visible light emission. When the binary digital baseband symbol is “1”, the driving circuit controls the LED to turn on and emit light; when the binary digital baseband symbol is “0”, the driving circuit controls the LED to turn off. Using this modulation method greatly reduces the design complexity of the modulation and demodulation circuit.

The LED driving circuit used in this work adds a carrier drawing-out circuit based on the basic common-source driving circuit to extract the remaining carriers in the junction capacitance when the LED is turned off, as shown in Figure 2a. The simple common-source circuit for the transistor MOS2 is used for driving the LED. The part surrounded by the dotted line is a carrier drawing-out part. U1 controls MOS1, and the signal of the inverse phase operation onto MOS2 is sent to MOS1. Hence, MOS1 is turned off at the time of the LED lighting and is turned on at the time of the LED turning off. Since both terminals of

the LED are short-circuited at the time of turning off, an LED remaining carrier is drawn out.

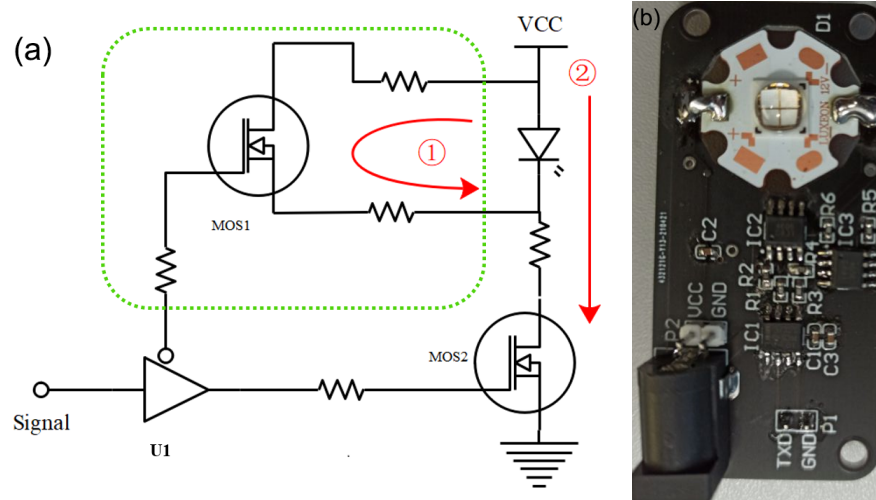


**Figure 2.** (a) The LED driver circuit. (b) Physical diagram of the transmitting circuit.

A commercial blue LED with a central wavelength of 450 nm is used as the light source for its large diffuse emission angle. Figure 3b shows the spatial distribution of the lights with royal blue and white, respectively. It can be seen that the blue light has a larger emission angle. In the underwater environment, the communication modem will inevitably have a certain jitter due to the influence of the water flow, and the large emission angle of the LED can reduce the probability of communication interruption and improve the robustness of optical communication.

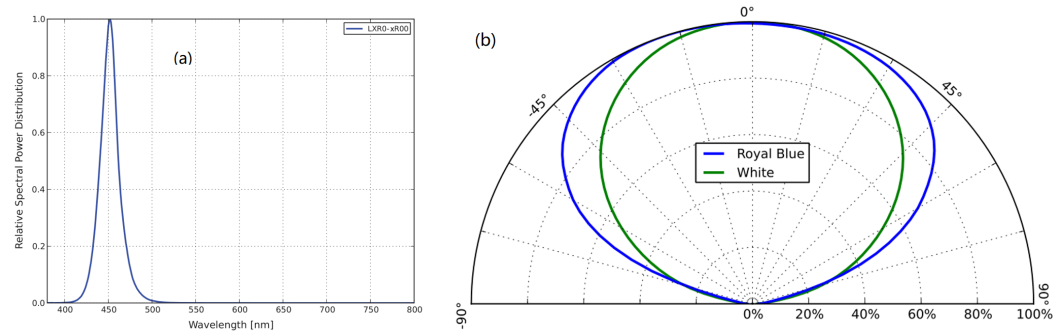


**Figure 3.** (a) LED wavelength characteristics. (b) Spatial distribution curve of radiation intensity.

### 2.2. VLC Receiver

The receiver, which is composed of the receiver front end, the signal shaping module, and the decision module, deals with the subsequent detection for further signal processing such as converting the visible light signal into an electrical signal, amplifying and filtering it to improve the signal-to-noise ratio, and obtaining the transformation of digital and analog signals. Finally, the receiver inputs the signal to the FPGA for subsequent decoding processing.

At the receiver, the modulated light is collected by a Fresnel lens, which is conducive to realizing UWVLC with a large field of view. Then, it converts the modulated light into an electronic current signal by a PIN photodiode, followed by a simple transimpedance amplifier (TIA) [20] to convert the current signal into a voltage signal. The  $-3$  dB cutoff frequency of the TIA is 5.05 MHz. In order to improve the modulation bandwidth of the VLC system, a first-order passive high-pass filter is inserted after the TIA, where the  $-3$  dB cutoff frequency is  $f_c \approx 1.064$  Mhz. After the filter, an amplifier circuit was designed to

amplify the filtered signal. The overall circuit design of the receiving part is shown in Figure 4.

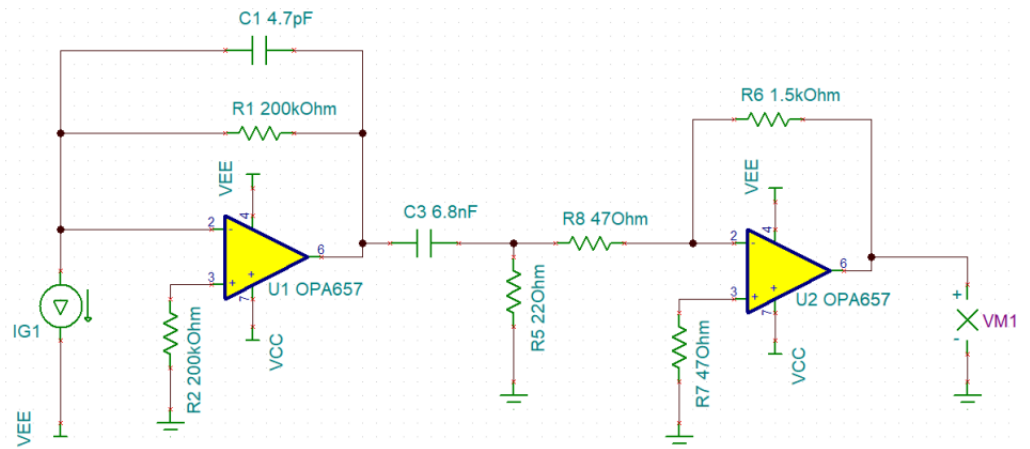


Figure 4. Receiver circuit diagram.

To match the TTL level standard of the IO input of the FPGA, a hysteresis comparator was designed at the last part of the VLC receiver, whose function is to convert the analog electrical signal into a digital rectangular wave signal. Compared with the open-loop comparator, the advantage of the hysteretic comparator is that it can shield the interference of the swing amplitude between the upper and lower threshold voltages. When the input signal varies between the lower threshold voltage  $V_{IL}$  and the upper threshold voltage  $V_{IH}$ , it will not cause the inversion of the output signal  $U_O$ ; when the input signal is above  $V_{IH}$  or below  $V_{IL}$ , the positive feedback introduced accelerates the transition of  $U_O$  and saturates the comparator output. The threshold voltage can be calculated according to Equations (1) and (2).

$$V_{IH} = \frac{R_1}{R_1 + R_2} V_{OH} \tag{1}$$

$$V_{IL} = \frac{R_1}{R_1 + R_2} V_{OL} \tag{2}$$

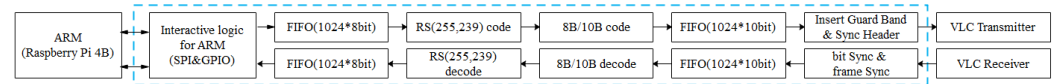
Decoupling capacitors are added to the power supply pins of all the operational amplifiers and comparator chips in the receiver to reduce the influence of the power supply noise on the signal. The final circuit diagram of the PCB is shown in Figure 5.



Figure 5. Visible light receiving circuit physical model.

### 2.3. FPGA and Signal Processing

In our work, the digital signal processing of the UWVLC system was designed based on the FPGA, as shown in Figure 6.



**Figure 6.** Schematic diagram of the FPGA data processing.

The functions implemented by the FPGA in the system include:

- Optical communication data is transmitted and received with raspberry PI based on the serial peripheral interface (SPI) protocol and the general purpose input/output (GPIO) port;
- The transmitting part performs Reed-Solomon (RS) encoding on the original data, and the receiving part performs RS(255,239) decoding on the 8B/10B decoded data;
- The transmitting part performs 8B/10B encoding on the RS-encoded data, and the receiving part performs 8B/10B decoding on the synchronized data.
- The transmitting part inserts a preamble and a synchronization header into the channel-encoded data; then, it performs the parallel-serial conversion and outputs it to the visible light signal transmitting circuit. The receiving part performs bit synchronization and frame synchronization on the digital binary signal after the ADC output by the visible light signal receiving circuit and outputs the 10-bit parallel signal after serial-parallel conversion.

In the designed optical communication system, the transmitter adds the timing pulse signal for bit synchronization and the frame synchronization header sequence for frame synchronization. The bit timing pulse signal is a periodic square wave signal in which “1” and “0” appear alternately, and the time width of each “1” and “0” signal is consistent with the time width of each bit in optical communication. The frame synchronization header adopts the 16-bit Barker code with sharp autocorrelation single peak characteristics [21]. In order to ensure the sampling time is in the middle of the received signal symbols, bit synchronization is required. The function of the frame synchronization module is to identify the 16-bit frame synchronization header in a frame of data and write the following data part into the First Input First Output (FIFO) memory.

The RS code [22] belongs to the forward error correction (FEC) method. It is a nonbinary Bose–Chaudhuri–Hocquenghem (BCH) code, and, of course, it also belongs to a cyclic code and a linear block code, which is especially suitable for dealing with burst errors. The purpose of using the RS code is to improve the reliability of channel transmission through redundant codes. In the system proposed in this paper, RS(255, 239) is used as the channel error correction code. The valid information of RS (255, 239) is 239 bits, and the check digit is 16 bits.

In the VLC system, if the modulated sequence has continuous “0” or continuous “1” for a long time, the energy ratio of the low-frequency part in the signal will be increased, which will increase the inter-symbol interference at the receiver, leading to a poor receiving eye diagram. These problems will eventually affect the clock recovery and timing judgment of the signal. In order to avoid this situation, the DC-balanced 8B/10B coding is introduced into the system [23]. The 8B/10B encoding converts every 8 bits in the data into 10 bits for output. In each group of 10 bits output, there will be no more than 6 bits of “1” or “0”, and no more than 5 consecutive “1” and consecutive “0” in the entire output data stream. By sacrificing 20% of the bit rate, 8B/10B coding ensures that the number of “1” and “0” in the entire data is balanced as much as possible. Most of the energy in the encoded data stream is concentrated in the high-frequency band, which effectively alleviates the inter-symbol interference and expands the receiving eye diagram.

#### 2.4. UAC Modem

The UAC modem adopts the ARM+DSP+FPGA architecture, which can realize dual-channel transmission and eight-channel reception. In this paper, in order to reduce energy consumption, only one channel of the communicator is used. However, the UAC modem must switch between sending mode and receiving mode through a switcher because it can only work in half-duplex mode. The underwater acoustic communication system parses the received signal and sends it to the Raspberry Pi through the serial port, which is further processed and forwarded to each module by the Raspberry Pi.

#### 2.5. Power Supply Module

Since the internal motor of the ROV uses a 12 V DC power supply, the UAC modem uses a 24 V DC power supply, and the operational amplifier and comparator are powered by  $\pm 5$  V voltage, the hardware system needs to convert the power supply. The system is powered by a 24 V lithium battery, and an EVEPS switching power supply module was selected to realize power isolation and 12 V regulated output. In the visible light receiving circuit part, the EVISUN IA1205S-1W switching power supply module was selected to realize the dual output of power isolation and voltage regulation. The nominal output ripple noise is  $30 \text{ mV}_{pp}$ , and the nominal switching frequency is 100 kHz. Moreover, in order to reduce the ripple noise, an LC filter circuit is attached to its 12 V voltage input terminal and  $\pm 5$  V voltage output terminal, as shown in Figure 7.

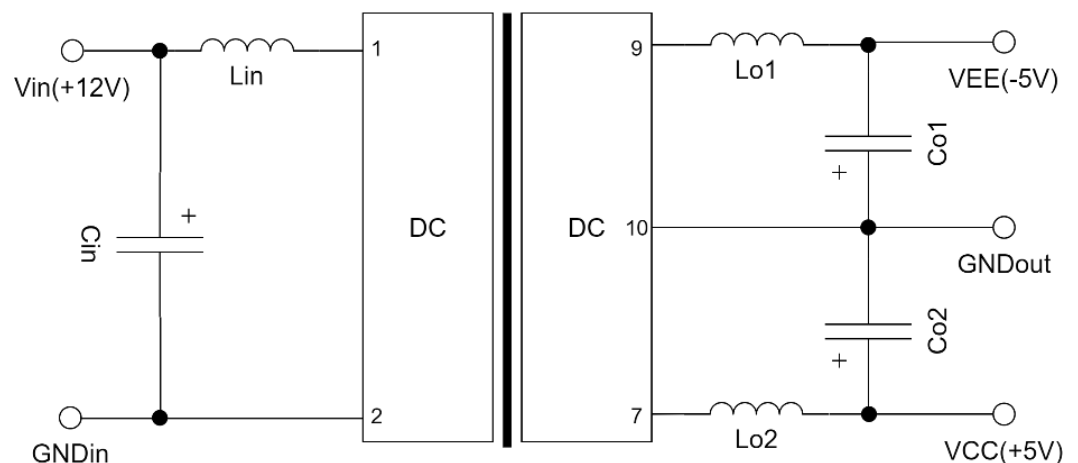


**Figure 7.** LC filter circuit.

#### 2.6. ROV Overview

An ROV is an underwater dynamic communication node, which can be used as the carrier of the VLC and UAC modems. At the same time, the ROV is also equipped with cameras, pressure sensors, attitude sensors, and voltage detection sensors to detect the underwater environment and its state. The overall structure of the ROV is shown in Figure 8. The structure has four horizontal thrusters and two vertical thrusters, which can ensure that the ROV has four degrees of freedom of motion capability: front and rear, left and right, heave, and horizontal rotation.

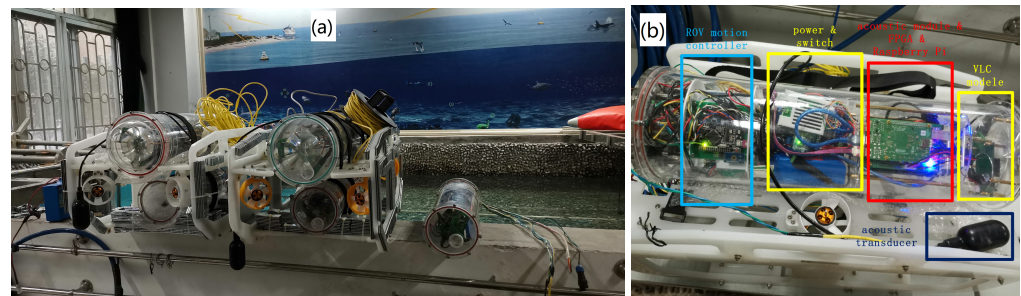


**Figure 8.** (a) ROV. (b) The internal structure of the ROV.

The ROV control system circuit was designed and developed by means of the module circuit assembly. This part of the system includes an Arduino microprocessor, pressure sensor, acceleration sensor, and DC brushless motor.

### 2.7. Transmission Protocol

In the actual UWVLC process, due to the interference of environmental factors such as underwater vehicle jitter and underwater turbulence, packet loss and bit errors will inevitably occur. In order to ensure an error-free transmission, we introduce an error retransmission mechanism to mark transmission error packets and lost packets at the receiver and feed them back to the transmitter for retransmission. The traditional ARQ protocols can be divided into three folds: Stop-and-Wait ARQ (SW-ARQ), Go-Back-N ARQ (GBN-ARQ), and Selective Repeat ARQ (SR-ARQ) [24]. In these traditional ARQ protocols, the uplink and downlink are usually equivalent. Furthermore, if they are directly applied to UWVLC, a series of problems will arise. First of all, the VLC has the characteristic of line-of-sight transmission, which requires strict link alignment [11,25]. In the application scenario of this paper, there is a dynamic communication node. If a bidirectional VLC link is introduced, the ROV control system requires extremely high precision, which is extremely difficult to implement. In addition, in order to ensure a larger receiving angle and a longer transmission distance, high-power LEDs and photoelectric sensors with higher sensitivity are often used in the system. The optical signal may interfere with its receiver due to backscattering. When the backscattered light is strong enough, the photoelectric sensor will be saturated or even damaged. Separating the transmitter and the receiver of the VLC and using a half-duplex communication mode can effectively solve the problem of backscattering interference [26]. When using the half duplex communication mode, the switching of transmission and reception modes will also reduce the throughput of the system.

The error-free data transmission protocol proposed for underwater optical–acoustic cooperative communication is based on our previous work [19], which we named Combinative-Selective-Repeat ARQ (CSR-ARQ). The protocol ensures error-free data transmission by separating the forward data transmission and backward ARQ data. The key motivation of the proposed CSR-ARQ scheme is to transmit high-speed data through visible light communication, while underwater acoustic communication transmits ARQ and low-speed control commands. Because the transmission media of the two communication methods are different, there is no problem with self-interference and backscattering. Since the downlink only needs to work in the simplex mode and does not need to establish a bidirectional optical link, the alignment requirements of the UWVLC link can be reduced, which is easy to implement in engineering.

“Combinative-Selective-Repeat” means combining multiple optical communication data frames into one packet. Since the length of the underwater acoustic communication data frame is only 42 bytes, the flag array for one feedback is limited. Therefore, by reorganizing multiple data frames into data packets the receiver can feedback the reception status of all data frames at one time. The working principle of CSR-ARQ is that the transmitter continuously sends data through visible light communication. After all data frames are sent, the receiver feeds back ARQ data packets through underwater acoustic

communication. In the ARQ data packet, the combined packet is the smallest unit. After receiving the ARQ packet, the transmitter determines whether to retransmit the data of the entire packet by analyzing the integrity of the corresponding packet location data. Until the next feedback comes, the transmitter will retransmit all the failed packets in a loop.

The mapping relationship between the underwater acoustic feedback data and optical communication data is shown in Figure 9. Since the underwater acoustic communication adopts the MFSK modulation method, which limits the data of each frame within the size range of 42 bytes, 42 bytes of data are used as a frame, in which the first byte is used as the frame header of protocol identification, and the remaining 41 bytes are used to represent the flags array of receiver reception. Since the corresponding data “/x00” will be recognized by the underwater acoustic communication module as the end symbol, and some eight bits of data corresponding to characters will be encoded as special symbols, this will result in data loss. Hence, it is not possible to directly use the bit “0” or “1” to represent the reception of the corresponding optical communication data packet position. In the protocol, considering the stability, we use one character to represent the position of five data packets, so 32 different characters are needed to represent all receiving states. Here, a total of 32 characters from “0” to “9” and “a” to “v” are mapped to 32 states from “00000” to “11111”, where “1” means successfully received, and “0” means not received. We use one character to represent the reception of five packets, then 41 bytes of data can represent a total of 205 packets. When the transmitter receives the ARQ data packet, it will retransmit the data packet marked “0”.

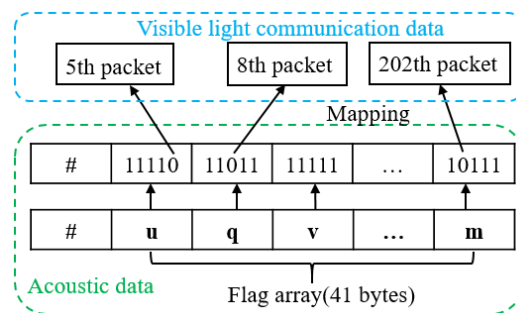


Figure 9. Data mapping relationship of CSR-ARQ.

### 3. Protocols’ Simulation

The CSR-ARQ protocols were simulated and compared with the traditional GBN-ARQ and SR-ARQ solutions [24,27]. In the existing works, the GBN-ARQ and SR-ARQ schemes were implemented using bidirectional links; that is, the uplink and downlink used the same medium. In this paper, as a comparison, the GBN-ARQ and SR-ARQ schemes used different links for uplink ARQ packets and downlink data; that is, the uplink used the underwater acoustic channel transmission and the downlink used the visible light channel transmission. The ultimate goal of the error-free data transmission protocol for optical–acoustic cooperative communication is to ensure the error-free transmission of UWVLC and improve the effective data throughput of visible light communication as much as possible under the condition of low-speed underwater acoustic ARQ feedback. The throughput of the ARQ systems is defined as the ratio of the total amount of data transmitted  $S$  (bits) to the time it takes to complete the transmission  $T$  (sec).

$$Throughput = \frac{S(bits)}{T(sec)} \tag{3}$$

In the simulation, we fixed the file size to 750 kB, set the packet loss rate from 0.001 to 0.5, and counted the time taken for the file to be transmitted without errors under different packet loss rates. Then we calculated the system throughput. It should be noted that the packet loss rate here refers to the ratio of the number of lost frames in the optical communication transmission data frame to the total number of transmission frames. For

CSR-ARQ, data frames were reassembled into packets, but the Packet Loss Rate set in the simulation was still the data frame loss rate. The average of 100 independent simulations is shown in Figure 10a.

The simulation results showed that the throughput of the CSR-ARQ scheme was significantly better than the GBN-ARQ scheme and SR-ARQ scheme, when the packet loss rate was in the range of 0.01–0.1. Furthermore, with the increase in the packet loss rate, the throughput of the CSR-ARQ scheme also dropped more gently. The throughput of the SR-ARQ scheme decreased significantly with the increase in the packet loss rate. This is because the flag array of the underwater acoustic feedback can only mark the positions of 13 unsuccessfully received data frames. That is, each feedback can only retransmit up to 13 data frames, which greatly limits the transmission efficiency.

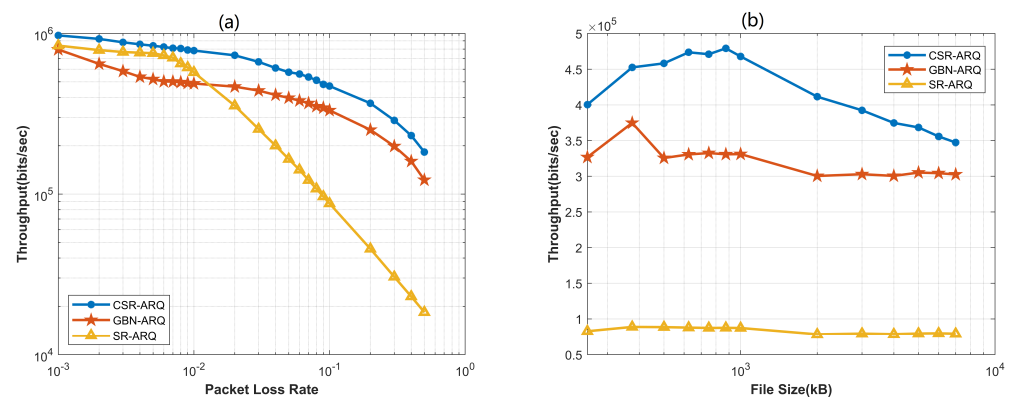


**Figure 10.** (a) When the file size is 750 kB, the throughput changes with the packet loss rate. (b) In the case of a packet loss rate of 0.1, the change in throughput with file size is shown.

In order to further investigate the impact of the transmission file size on different schemes, we set the packet loss rate to 0.1. Figure 10b shows the results of the throughput of each scheme as a function of the file size.

It can be seen that in the case of different file sizes, the throughput of the CSR-ARQ scheme was better than that of the GBN-ARQ scheme and the SR-ARQ scheme, and its peak value was in the range of file sizes of 750–1000 kB. However, when the file size exceeded 1000 kB, the throughput of the CSR-ARQ solution decreased significantly as the file increased, while the throughput curve of the other two solutions was relatively stable. The reason is that these two schemes do not re-combine optical communication data frames compared with CSR-ARQ. This approach enables it to accurately locate the location of the lost packets and does not change with the file size, but this is at the expense of the number of lost packets. The location of packet loss in the CSR-ARQ solution was relatively ambiguous, and the location accuracy varied with the file size. Limited by the length of the underwater acoustic communication data frame, the SR-ARQ scheme could only obtain the positions of 13 missing packets in one feedback, and the efficiency was severely restricted.

#### 4. Experiment

The experiment was conducted in the laboratory pool (7 m  $\times$  5 m  $\times$  1.3 m), as shown in Figure 11. The experiment mainly analyzed the output waveform of the transmitting circuit, the receiving eye diagram, and the relationship between the offset angle and the bit error rate.



Figure 11. Laboratory pool environment.

#### 4.1. Transceiver Circuit Signal Test

As discussed in the paper [28], the received power varies linearly with the transmitted power. Therefore, the optical power of the receiver can be improved by increasing the photoelectric conversion efficiency of the transmitter. To analyze the output waveform of the transmitting circuit, we used a signal source to generate a square wave signal with a frequency of 5 MHz and a duty ratio of 1:1 into the signal terminal of the circuit and used an oscilloscope to observe the voltage signal on the negative pole of the LED. A simple common-source circuit was used as a control group. The test waveform is shown in Figure 12.



Figure 12. LED negative voltage signal.

It can be seen from the figure that after adding the carrier drawing-out circuit, the voltage of the LED dropped rapidly to 0 V when it was turned off, and the signal peak-to-peak value loaded on the positive and negative poles of the LED reached 10.7 V, while the effective signal peak of the basic common source drive circuit was only 1.2 V. The experimental results showed that the circuit realized the function of extracting the remaining carriers in the LED junction capacitance. Figure 13 shows the effective signal strength of the positive and negative voltages of the LED driven by different frequency signals.

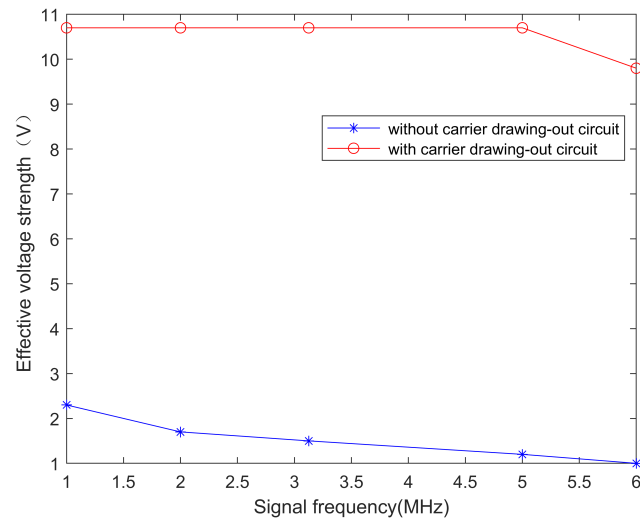


**Figure 13.** The effective signal strength of LED positive and negative voltages driven by different frequency signals.

We combined the transmitting circuit with the receiving circuit for debugging. The transmitter input the PN15 pseudo-random sequence “111100010011010” with a frequency of 5 Mbps through the signal generator and observed the final output signal of the receiver. The obtained eye diagram is shown in Figure 14. It can be seen that when the frequency of the transmitted signal was 5 MHz, the degree of eye-opening was large, and the inter-symbol interference was not obvious. The experimental results show that the transmitter circuit can realize visible light communication with a bit rate of 5 Mbps, which meets the requirements of underwater real-time picture and video transmission.

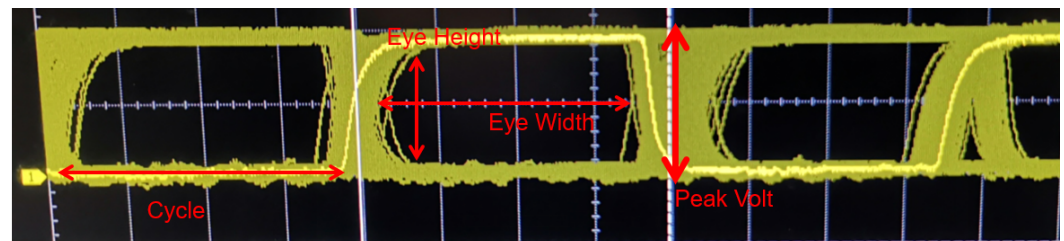


**Figure 14.** Receiver output eye diagram.

#### 4.2. Bit Error Rate for Visible Light Communication

The underwater optical communication node installed in the ROV was used as the receiver, and the communication node installed in the static underwater sealed cabin WAS used as the transmitter. To test the BER of point-to-point UWVLC under static conditions, each test sent 50,000 data packets with fixed text sequences, and the effective data length in each data packet was 239 bytes. Then receiver calculated the BER, where each symbol was 1 byte, and the RS code was not added during the experiment. Considering that the VLC modem in the ROV will inevitably be disturbed by environmental factors such as the movement of the vehicle, it is difficult to achieve the accuracy of manual alignment of the optical communication link in the actual environment. Therefore, we tested the BER of optical communication with a fixed distance of 7.6 m and the transmitter pointing at different angles. During the experiment, the direction of the receiver was fixed. We used the laser pointer to realize the initial alignment to ensure that the receiver and the transmitter were on the same line, and then gradually increased the offset angle in the direction of the transmitter. The test results are shown in Figure 15.

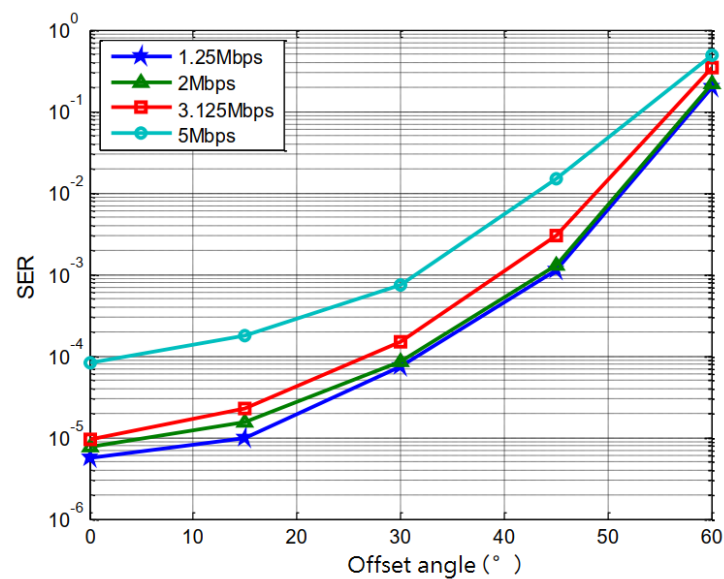


**Figure 15.** The BER at different transmitter offset angles.

It can be seen that with the increase in the offset angle, the BER gradually increased. This is because the radiation intensity of the LED decreased with the increased offset angle, which reduced the optical power received. At the 5 Mbps data rate, the BER was significantly higher than the other three rates at the same angle. This is because the  $-3$  dB bandwidth of the PD S6801 used in the receiving circuit is low, and the photoelectric conversion efficiency is reduced at 5 MHz frequency. In the actual system, the error rate of the final received information is generally reduced by error correction coding. Under the above experimental conditions, we set the offset angle of the transmitter to  $30^\circ$ , the offset angle of the receiver to  $0$ , and added RS(255, 239) coding to the system. The BER measured in the experiment is as shown in Table 1:

**Table 1.** Experimental results of the bit error rate at different transmission rates.

Rate	BER
1.25 Mbps	0
2 Mbps	0
3.125 Mbps	0
5 Mbps	$7.53 \times 10^{-7}$

The experimental results show that the designed UWVLC system can obviously improve the BER when the error rate is low by adding error correction codes. At a transmission rate of 5 Mbps, the system can achieve reliable communication with a BER lower than  $10^{-6}$  within an angular difference of  $\pm 30^\circ$  between the transceiver and the transceiver at a distance of at least 7.6 m in clear water.

#### 4.3. Outdoor Test

In order to further verify the system performance, we tested the communication distance of the system in a pool with high green algae content, and the test environment is shown in Figure 16. It can be seen that the chlorophyll content in the pool was relatively high, and there were many impurities in the water.



**Figure 16.** Outdoor pool environment.

When the transmitter and receiver were aligned (the offset angle did not exceed  $10^\circ$ ) and the RS (255,239) error correction code was added, the results of the maximum communication distance without errors for each transmission rate are shown in Table 2:

**Table 2.** The maximum transmission distance without errors at each transmission rate.

Rate	Distance
1.25 Mbps	6 m
2 Mbps	5.8 m
3.125 Mbps	5.4 m
5 Mbps	3.6 m

The results show that the maximum communication distance of the system in the turbid pool was much shorter than that of the indoor pool. According to the paper [29], chlorophyll has the most serious attenuation to visible light with a wavelength of about 430 nm. Further, considering the impurities in the water, it is normal for the visible light to attenuate seriously.

In this turbid pool, we set the transmission rate to 3.125 Mbps, and collected the voltage strength of the received signal (the average peak-to-peak value of the received signal voltage) at different distances. The results are shown in Figure 17. The curve in the figure was fitted according to the optical power attenuation formula (4) at the receiving end in seawater.

$$P_r = P_t \times e^{-c(\lambda)d} \quad (4)$$

where  $P_t$  is the transmitted signal power,  $P_r$  is the received signal power,  $d$  is the communication distance, and the attenuation coefficient of 450 nm wavelength visible light in the turbid pool is about  $c(\lambda) = 0.3299$ . According to the paper [10], the attenuation coefficient in deep-sea clear water is 0.151, and the error-free communication distance of the system at a communication rate of 3.125 Mbps can reach 11.8 m.

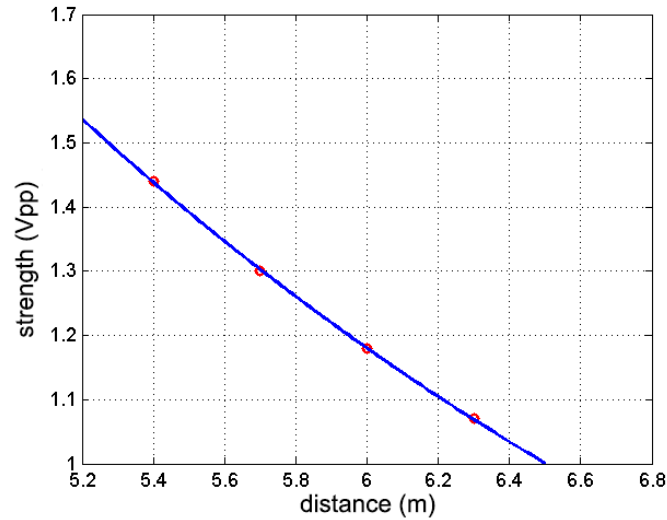


Figure 17. The received signal strength varies with the communication distance.

4.4. Error-Free Data Transmission Test for Optical–Acoustic Cooperative Communication

It can be seen from the previous experimental results that the bit error rate performance of the underwater optical communication system was greatly affected by the receiver’s offset angle, and the effective receiving field angle of the receiver without bit error was small. Through the CSR-ARQ optical-acoustic cooperative communication protocol, error-free data transmission can be realized under the condition of only establishing a one-way optical communication link, which reduces the requirements for alignment accuracy of the optical communication system.

We carried out field experiments in a laboratory pool. In the experiment, the optical communication transmission rate was set to 2 Mbps, and the transmission file was a picture with a size of about 783 kB. Ten groups of transmission experiments were carried out, and the ROV was relocated to a new position in each experiment. The experimental results are shown in Figure 18.

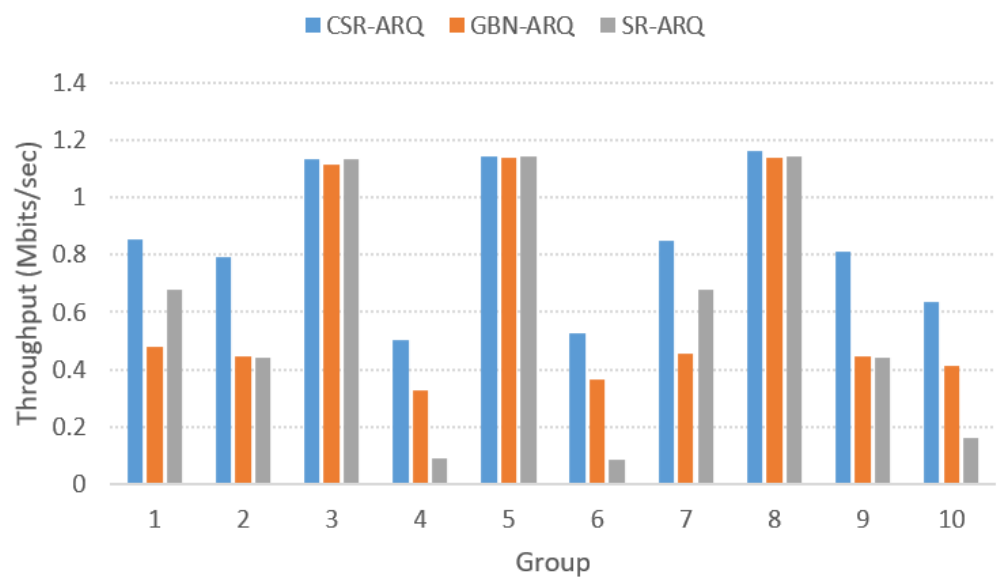


Figure 18. The throughput test results of each error-free data transmission scheme.

According to the data in Figure 18, the throughput of the system was higher after adopting the CSR-ARQ protocol. The throughput of the SR-ARQ solution was relatively low, which we could also predict from the analysis of the simulation. We counted the number of frames sent by the transmitter and the number of frames received by the receiver in the first 5 s of each program experiment and analyzed the current packet loss rate of each group of experiments. It was found that the packet loss rates of the third, fifth, and eighth groups were close to 0. In this case, all ARQ protocols were almost ineffective, so the throughput of each scheme was almost the same. Table 3 shows the statistical results of the packet loss rate of group 6 and group 9. The packet loss rates of both groups were less than 10%, and the experimental results were close to the simulation results.

**Table 3.** The packet loss rate in the experiment.

Group	CSR-ARQ	GBN-ARQ	SR-ARQ
6	0.1002	0.1005	0.1030
9	0.0143	0.0123	0.0172

The experimental results show that the underwater optical-acoustic cooperative communication system designed in this paper can realize the error-free data transmission of a 2 Mbps communication rate within 7.6 m distance of the indoor clear pool. The CSR-ARQ scheme proposed in the paper had the best performance under the file sizes of 750–1000 kB. In practice, large-capacity data files can be split into subfiles within this range, and the CSR-ARQ scheme can be used for segmented and reliable transmission.

## 5. Conclusions

In this paper, we constructed an underwater optical–acoustic cooperative communication platform for underwater wireless data transmission and applied it to an ROV. A series of simulations and experiments were designed to verify the performance of the system, such as the output waveform of the visible light communication transmitter circuit, the receiver eye diagram, the outdoor communication distance, and the optical–acoustic cooperative communication data transmission.

The performance of underwater visible light communication depends on many factors, such as transmit power, underwater attenuation coefficient, transmission rate, and offset angle. For simplicity, we chose the classical OOK modulation scheme in the system. In the data processing, we introduced RS coding and 8B/10B coding to reduce the BER.

We also proposed an error-free data transmission protocol for optical–acoustic cooperative communication to ensure the accurate transmission of underwater data. High-speed data such as images and video are transmitted through visible light communication, while low-speed data such as control signaling are transmitted through acoustic communication. The performance of the underwater optical–acoustic cooperative communication system was proved to be satisfactory according to the experimental results.

The angular offset of the transmitter and receiver has a large impact on the performance of the system. The experiment was implemented in a stationary environment with fixed underwater nodes. In a dynamic environment, the link alignment of visible light communication will have a large impact on the system. Further work should investigate the automatic alignment of visible light links in dynamic environments. In addition, further research on optical–acoustic cooperative wireless communication using this system is expected in both shallow and deep seas.

**Author Contributions:** Conceptualization, X.Z. and F.C.; methodology, X.Z.; software, J.H., J.L., and S.X.; validation, J.H., J.L., and F.C.; formal analysis, X.Z.; investigation, J.L.; resources, S.X.; data curation, J.H.; writing—original draft preparation, J.H.; writing—review and editing, X.Z., J.L., and F.C.; visualization, S.X.; supervision, J.L.; project administration, F.C.; funding acquisition, X.Z. All authors have read and agreed to the published version of the manuscript.

**Funding:** This work was financially supported by the Science and Technology Program of Guangdong Province, China (Grant No.: 2018B020207002).

**Conflicts of Interest:** The authors declare no conflict of interest.

## References

1. Constantinos, T.; Thierry, B.; Al, M.A. Seafloor seismic acquisition using autonomous underwater vehicles. *Geophys. Prospect.* **2019**, *67*, 1557–1570.
2. Simetti, E.; Indiveri, G.; Pascoal, A.M. WiMUST: A cooperative marine robotic system for autonomous geotechnical surveys. *J. Field Robot.* **2021**, *38*, 268–288. [[CrossRef](#)]
3. Reddy, V.A.; Stüber, G.L. Wi-Buoy: An Energy-Efficient Wireless Buoy Network for Real-Time High-Rate Marine Data Acquisition. *IEEE Access* **2021**, *9*, 130586–130600. [[CrossRef](#)]
4. Zhu, S.; Chen, X.; Liu, X.; Zhang, G.; Tian, P. Recent Progress in and Perspectives of Underwater Wireless Optical Communication. *Prog. Quantum Electron.* **2020**, *73*, 100274. [[CrossRef](#)]
5. Khalighi, M.A.; Uysal, M. Survey on Free Space Optical Communication: A Communication Theory Perspective. *Commun. Surv. Tutor. IEEE.* **2014**, *16*, 2231–2258. [[CrossRef](#)]
6. Khalighi, M.A.; Gabriel, C.; Hamza, T.; Bourennane, S.; Rigaud, V. Underwater Wireless Optical Communication; Recent Advances and Remaining Challenges. In Proceedings of the 2014 16th International Conference on Transparent Optical Networks (ICTON), Graz, Austria, 6–10 July 2014; pp. 1–4.
7. Son, H.J.; Choi, H.S.; Tran, N.H.; Ha, J.H.; Ji, D.H.; Kim, J.Y. Study on underwater wireless communication system using LED. *Mod. Phys. Lett. B* **2015**, *29*, 1540023. [[CrossRef](#)]
8. Kumar, P.; Trivedi, V.K.; Kumar, P. Recent trends in multicarrier underwater acoustic communications. In Proceedings of the 2015 IEEE Underwater Technology (UT), Chennai, India, 23–25 February 2015; pp. 1–8.
9. Gussen, C.; Diniz, P.; Campos, M.; Martins, W.; Costa, F.; Gois, A. A Survey of Underwater Wireless Communication Technologies. *J. Commun. Inf. Syst.* **2016**, *31*, 242–255. [[CrossRef](#)]
10. Kaushal, H.; Kaddoum, G. Underwater Optical Wireless Communication. *IEEE Access.* **2016**, *4*, 1518–1547. [[CrossRef](#)]
11. Tang, S.; Dong, Y.; Zhang, X. On Link Misalignment for Underwater Wireless Optical Communications. *IEEE Commun. Lett.* **2012**, *16*, 1688–1690. [[CrossRef](#)]
12. Vasilescu, I.; Varshavskaya, P.; Kotay, K.; Rus, D. Autonomous Modular Optical Underwater Robot (AMOUR) Design, Prototype and Feasibility Study. In Proceedings of the 2005 IEEE International Conference on Robotics and Automation, Barcelona, Spain, 18–22 April 2005; pp. 1603–1609.
13. Farr, N.; Ware, J.; Pontbriand, C.; Hammar, T.; Tivey, M. Optical communication system expands CORK seafloor observatory’s bandwidth. In Proceedings of the OCEANS 2010 MTS/IEEE SEATTLE, Seattle, WA, USA, 20–23 September 2010; pp. 1–6.
14. Pontbriand, C.; Farr, N.; Hansen, J.; Kinsey, J.C.; Fourie, D. Wireless data harvesting using the AUV Sentry and WHOI optical modem. In Proceedings of the OCEANS 2015-MTS/IEEE, Washington, DC, USA, 19–22 October 2015 ; pp. 1–6.
15. Hansen, J.; Fourie, D.; Kinsey, J.C.; Pontbriand, C.; Tivey, M. Autonomous acoustic-aided optical localization for data transfer. In Proceedings of the OCEANS 2015-MTS/IEEE Washington, Washington, DC, USA, 19–22 October 2015; pp. 1–7.
16. Han, S.; Noh, Y.; Liang, R.; Chen, R.; Cheng, Y.J.; Gerla, M. Evaluation of Underwater Optical-Acoustic Hybrid Network. *China Commun.* **2014**, *11*, 49–59.
17. Han, S.; Noh, Y.; Lee, U.; Gerla, M. Optical-acoustic Hybrid Network Toward Real-time Video Streaming for Mobile Underwater Sensors. *Ad Hoc Netw.* **2018**, *83*, 1–7. [[CrossRef](#)]
18. Zhang, D.; N’Doye, I.; Ballal, T.; Al-Naffouri, T.Y.; Alouini, M.-S.; Laleg-Kirati, T.-M. Localization and tracking control using hybrid acoustic-optical communication for autonomous underwater vehicles. *IEEE Internet Things J.* **2020**, *7*, 10048–10060. [[CrossRef](#)]
19. He, J.; Wu, J.; Peng, Z.; Chen, F.; Yu, H.; Ji, F. Underwater Error-Free Data Transmission Based on Optical-Acoustic Cooperative Communication. In Proceedings of the 2021 IEEE/CIC International Conference on Communications in China (ICCC Workshops), Xiamen, China, 28–30 July 2021; pp. 211–216.
20. Sun, L. Relationship between S-parameters and Trans-impedance Gain of Transimpedance Amplifiers. *Res. Prog. SSE Solid State Electron.* **2006**, *26*, 85–90.
21. Hossain, M.A. Performance Analysis of Barker Code Based on their Correlation Property in Multiuser Environment. *Int. J. Inf. Sci. Tech.* **2012**, *2*, 27–39. [[CrossRef](#)]
22. Reed, I.S.; Solomon, G. Polynomial Codes Over Certain Finite Fields. *J. Soc. Ind. Appl. Math.* **1960**, *8*, 300–304. [[CrossRef](#)]
23. Widmer, A.X.; Franaszek, P.A. Transmission code for high-speed fibre-optic data networks. *Electron. Lett.* **1983**, *19*, 202–203. [[CrossRef](#)]
24. Shu, L.; Costello, D.J.; Miller, M.J. Automatic-repeat-request error-control schemes. *IEEE Commun. Mag.* **1985**, *22*, 5–17.
25. Zhang, H.; Dong, Y. Link misalignment for underwater wireless optical communications. In Proceedings of the 2015 Advances in Wireless and Optical Communications (RTUWO), Riga, Latvia, 5–6 November 2015; pp. 215–218.
26. Han, B.; Zhao, W.; Meng, J.; Zheng, Y.; Yang, Q. Study on the backscattering disturbance in duplex underwater wireless optical communication systems. *Appl. Opt.* **2018**, *57*, 8478–8486. [[CrossRef](#)] [[PubMed](#)]

27. Gao, M. A Transmission Scheme for Continuous ARQ Protocols over Underwater Acoustic Channels. In Proceedings of the 2009 IEEE International Conference on Communications, Dresden, Germany, 14–18 June 2009; pp. 1–5.
28. Wang, P.; Chao, L.; Xu, Z. A Cost-Efficient Real-Time 25 Mb/s System for LED-UOWC: Design, Channel Coding, FPGA Implementation, and Characterization. *J. Light. Technol.* **2018**, *36*, 2627–2637. [[CrossRef](#)]
29. Prieur, L.; Sathyendranath, S. An optical classification of coastal and oceanic waters based on the specific spectral absorption curves of phytoplankton pigments, dissolved organic matter, and other particulate materials. *Limnol. Oceanogr.* **1981**, *26*, 671–689. [[CrossRef](#)]